Automated Reference Points Selection for InSAR Time Series Analysis on Segmented Wetlands in California

Boya Zhang, Erin Hestir, Zhang Yunjun, *Member, IEEE*, Matthew E. Reiter, Joshua H. Viers, Danica Schaffer-Smith, Kristin Sesser, Talib Oliver-Cabrera

Abstract— **Interferometric Synthetic Aperture Radar (InSAR) time series analysis is a powerful technique to estimate long-term water level changes in wetlands ecosystems. However, few studies have applied InSAR on wetlands that are highly segmented by canals and levees due in part to the challenge of selecting qualified reference points to minimize unwrapping errors, which, by contrast, is a relatively easy task for unsegmented wetlands. Here we developed a new method to automatically select the optimal reference point for InSAR time series analysis. The method selects reference points by considering temporal behaviors of coherence and InSAR phase connectivity from each reference point to its wetland of interest. We tested the method on six managed and highly segmented wetland units within the Sacramento National Wildlife Refuge in the Central Valley, California. We validated the InSAR measurement against water depth gauge measurements during a low water depth (<10 cm) period from 2016 to 2018. The overall accuracy of the estimated water depth changes achieved an RMSE of 1.60 cm. Compared with the traditional method of manually selecting a single reference point for all wetland units with an overall RMSE of 1.82 cm, our method showed significantly lower RMSE values (p-value < 0.05) for five out of six units and similar RMSE for the remaining one. This new automatic method enables us to maximize the performance of InSAR to predict water depth and could be applied to other types of InSAR applications as well.**

Index Terms— **coherence, connected component, reference point, water depths, wetland InSAR**

B. Zhang, E. Hestir, and J. Viers are with the School of Engineering, University of California Merced, Merced, CA, USA (email:bzhang64@ucmerced.edu).

Z. Yunjun is with the Seismological Laboratory, California Institute of Technology, Pasadena, CA 91125 USA.

M. Reiter and K. Sesser are with Point Blue Conservation Science, Petaluma, CA, USA.

D. Schaffer-Smith is with the Nature Conservancy, Durham, NC, USA.

T. Oliver-Cabrera is with the Jet Propulsion Laboratory, California Institute of Technology, Pasadena, CA 91109 USA. (*This work was done as an outside activity and not in the author's capacity as an employee of the Jet Propulsion Laboratory, California Institute of Technology.*)

I. INTRODUCTION

Interferometric Synthetic Aperture Radar (InSAR) has been successfully applied to estimate water level variations in both managed and natural wetlands [1-6]. This application of remote sensing technology is most effective in wetlands with emergent herbaceous and woody vegetation with vertical structures above water surfaces, which enables double-bounce scattering [1-3]. Early studies used phase differences measured by a pair of SAR observations to estimate water level change between two snapshots in time [1-3]. To satisfy the need of wetland management for continuous monitoring of water levels, recent studies used advanced time series analysis, such as small baseline subsets (SBAS), to estimate water level variation across an extended time window (e.g., years) [5]. One of the critical steps for those InSAR applications is to select reference points with high and stable coherence over time and close to the target area, such as nearby residential areas [2]. Previous studies used a single reference point for wetlands of interest because they only focused on natural wetlands or managed wetland units with limited spatial segmentation [1-3], and thus only needed one stable point outside the wetland area.

However, the single reference point method may fail for highly segmented wetlands with distinct hydrologic regimes because of (1) unwrapping errors among different wetland units and (2) decorrelation areas of vegetation that obstruct a coherent path from the reference location to the wetland of interest [6]. While multi-segment processing (each segment with its own local reference point) recently proposed by Kang et al. (2021) could mitigate the impact of decorrelation [7], it still requires manual reference point selection, which can be tedious and challenging even for experts.

Our study developed an automatic reference point selection method for multi-temporal InSAR applications. The method considers the location, coherence, and phase connectivity between the reference and wetland unit to maximize the phase connectivity between the two, thus, minimizing the impact of unwrapping errors. We tested the method using highly segmented managed wetlands with areas much smaller than those of previous studies [1-6]. The method builds upon the connected components from the phase unwrapping process and can be incorporated into open-source InSAR time series analysis packages, such as MintPy [8]. We tested the method using a C-band Sentinel-1 InSAR dataset over six segmented wetland units, where water depth gauge data were available, located within the Sacramento National Wildlife Refuge (Sacramento Refuge) in the Central Valley of California, USA (Fig. 1(a)). This method can select an optimal reference for each unit. We compared water depth estimates from this automated reference point selection to water depth estimates made using the traditional, manual reference point selection method. Since most wetlands in California are managed with limited

information on water depth, which often differs among units, this study meets the urgent need to assist wetland resource managers in monitoring surface water depth.

II. STUDY AREAS AND DATASETS

Managed wetlands in California provide important services such as supporting millions of shorebirds and waterfowl during their non-breeding season [9-10]. The Sacramento Refuge, primarily made up of emergent non-tidal wetlands, is located in the northern half of the Central Valley, which is a critical part of the Pacific Flyway, hosting one of the largest concentrations of migratory birds in the world during fall and winter [10]. The wetland hydrology is characterized by a seasonal pattern (Fig. 1(b)) of flooding and drawdowns, scheduled to mimic historical dry and wet seasonality and facilitate waterfowl management in the winter and spring seasons. The wetland units are intentionally flooded from fall through spring, i.e., the wet season, from October to March [9]. The source of the flooding is subject to local rainfall and water allocation decisions by refuge managers. The Sacramento Refuge wetlands are highly segmented with a total number of 196 units across 4000 ha, with an average of ~20 ha per unit (Fig. 1(a)). We tested the reference point selection method described below using six wetland units (Fig. 1(a)), each outfitted with a pressure transducer water level gauge measuring sub-daily water depth from December 2016 to May 2018. We obtained 10-m Digital Terrain Models (DTM) for each unit generated by the previous study via Real-Time Kinematic Survey [9].

The Sentinel-1 satellite constellation operates in C-band and works in all weather conditions, day and night. This study used Sentinel-1 Interferometric Wide (IW) mode Single Look Complex (SLC) products with 250 km wide swath and pixel spacing of 2.3 m by 14.1 m in range and azimuth directions, respectively. The revisit period for each Sentinel-1 satellite is 12 days. Sentinel-1 provides VV and VH polarizations for the study areas, but we only used VV for analysis, which showed better performance in interferometry than VH [3]. We obtained 43 scenes (including Sentinel-1A and 1B) from descending path 115, covering from December 24, 2016 to May 13, 2018, which overlapped with measurements of water depths (Fig. 1(b)).

We processed the time series of Sentinel-1 repeat-pass SAR acquisitions to form sets of coregistered unwrapped interferograms, including unwrapped phase, coherence, and connected components, by employing the ISCE-2 stack Sentinel processor and SNAPHU phase unwrapping [11-13]. We connected each SAR acquisition with its nearest two neighbors. For each interferogram, we applied a Goldstein filter with a strength of 0.8, and a multilooking with a factor of two and six in azimuth and range directions, respectively. We geocoded the output products into the WGS84 coordinate system and resampled to a ~30 m grid. We used only the dry season when water depths were lower than 10 cm because high water levels and high variations lead to greater
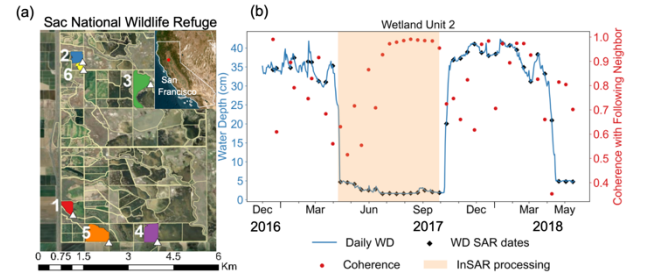

Fig. 1. (a) Location of the Sacramento Refuge. (b) Unit boundaries (yellow), six units with water depth data, and water gauges (white triangles). (c) Time series of daily mean water depth of Unit 2 (left axis, blue line), measurements corresponding to SAR acquisitions (dark diamonds), and InSAR coherence value (between current and following adjacent observation, right axis, red dot).

unwrapping errors, which makes it difficult to test the algorithm. The low water-depth period is from April to October, and it can be slightly different between different units.

III. METHODOLOGY

Given a given Area of Interest (AOI, in this case, a wetland unit), the method automatically selects the reference point as a part of the procedure in InSAR time series analysis. The main goal of the method is to find optimal reference points that satisfy three criteria: (1) located outside but close to a wetland unit, (2) have high coherence values over time, and (3) have a coherent path, i.e., spatially adjacent pixels with high coherence values, from the reference to the AOI.

Data preparation obtains several products from Terrain Observation with Progressive Scan (TOPS) stack processing. The unwrapped phase (the yellow rectangle outlined by a dashed line in the Data Preparation step of Fig. 2(a)) is not used in the reference selection method but is used in later steps of InSAR processing. The reference selection method also requires a user-supplied geographic delineation of an AOI (e.g., shapefile data, Fig. 2(a)) with the same coordinate system (WGS84) as InSAR data. The method can be described as a five-step procedure as below.

Step 1 labels the pixels using the AOI shapefile. Pixels outside of the AOI are labeled as 0 and those within as 1. For this study, the method selects reference candidates outside the AOI (a wetland unit) because selecting a reference within the AOI cancels out displacement signals due to homogeneous water level changes in space.

Step 2 selects reference pixel candidates based on coherence values in time. This step identifies pixels with spatial coherence values greater than threshold *coh_thd* (initial value of 0.9) for more than *perc_thd* (initial value of 95%) of InSAR pairs in time (blue patches in Fig. 3(a)).

Step 3 evaluates phase connectivity using a pixel-level iterative searching process for each pixel within an AOI. This step evaluates phase connectivity using the percentage of InSAR pairs that an AOI pixel's connections to a nearby reference candidate obtained from Step 2 using the connected component output from the data preparation step (Fig. 2(a)). For a connected component image, zero values indicate no
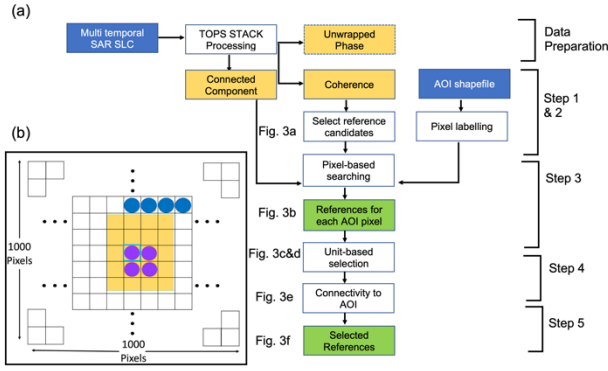
Fig. 2. (a) Flowchart of the five-step procedure. (b) Schematic plot for Step 3. The search grid is centered at a pixel within the AOI (with a light green square). Orange grids represent the extent of an AOI; purple pixels are pixels within the AOI; blue pixels are outside of the AOI.

TABLE I
Initial threshold parameters used in this study

Parameters	Initial	Parameters	Initial
coh_thd	0.9	*quality_thd*	30
perc_thd	0.95	*min_area*	30
edge	1000	*px_per_comp*	5
conn_perc_thd	0.8	*path_thd*	0.9

connection with neighbor pixels, and pixels sharing the same positive values are connected. For each AOI pixel, this step searches for surrounding reference candidates within a square with an edge length of 1000 pixels (*edge* parameter in Table 1), i.e., ~3000 m, which covers almost the entire Sacramento Refuge (Fig. 3(b)). For a reference candidate within the square (e.g., the cyan dot in Fig. 3(b)), if the percentage of connections to the AOI pixel is greater than a *conn_perc_thd* threshold (initial value of 0.8), we identify it as a reference candidate (red, yellow, and green dots in Fig. 3(b)). As a result, each AOI pixel has a list of reference candidates.

Step 4 selects reference points at the AOI level. To remove noisy AOI pixels (e.g., open water), we remove AOI pixels with less than *quality_thd* (initial value of 30) reference candidates. We intersect the reference candidate lists for all remaining AOI pixels to obtain a list of reference candidates that have high connections with all qualified AOI pixels (Fig. 3(c)). If this step does not find any reference points, tuning of the *perc_thd* and *conn_perc_thd* parameters is required. Considering coherence is the priority for reference selection, parameter tuning prioritizes decreasing *conn_perc_thd*. We use an increment of 0.5 for both parameters.

Step 4 conducts a connected component analysis to represent different locations of clusters of the reference candidates (Fig. 3(d)). A *min_area* threshold (initial value of 30) is applied to remove clusters with a low number of candidates. For each component, we selected the top
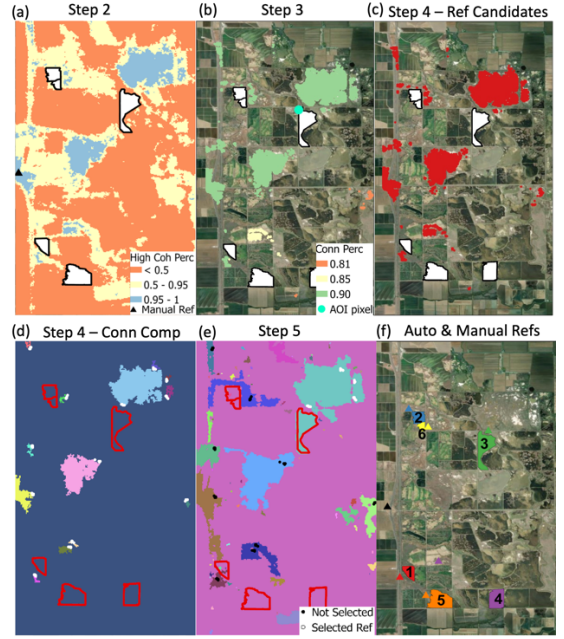

Fig. 3. Intermediate results for each step using Unit 3 as an example. (a) Percentage of high coherence in time. (b) Percentage of connections to the AOI pixel (cyan dot). (c, d) Selected reference candidates and connected components representing different locations. (e) Connected component based on mean coherence value (pink color is the background with a zero value) with selected and unselected reference points. (f) Locations of reference for each unit and the manually selected reference point (black triangle).

px_per_comp (initial value of 5) candidates with the shortest distance to the AOI (white dots, Fig. 3(d)).

Step 5 considers a coherent path between the reference candidates to the AOI. First, we generate a mask image based on a mean coherence image of all InSAR pairs using a threshold *paththd* (initial value of 0.9). The mask consists of 1 and 0 values, representing mean coherence greater or smaller than *paththd*, respectively. We mark all the AOI pixels as 1 before conducting a connected component analysis for the mask image. For the reference obtained from Step 4 sharing the same connected component with the AOI pixels (Unit 3 and nearby component in Fig. 3(e)), meaning a coherence path exists between the candidate to the AOI, we select those as final reference points and rank them by the Euclidean distance to the AOI (the top one has the shortest distance). If the AOI is not connected to any component, we conduct an incremental dilation (step of 1) to surrounding pixels until the AOI is connected to a component.

IV. RESULTS

We applied the method to each of the six wetland units in Sacramento Refuge and calculated water depth variation based on selected reference points. Results from the applied method showed (1) the predicted water depth from InSAR compared to the ground reference (Fig. 4), and (2) the comparison between our automated method and a manually selected single reference point in terms of accuracy for the estimated water depths (Fig. 5, 6).
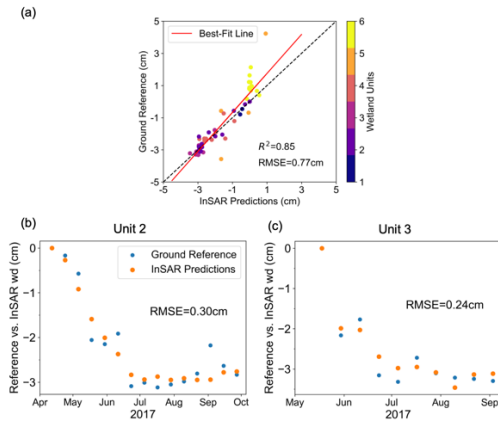
Fig. 4. (a) Comparison between InSAR-derived water depths and ground reference using a representative pixel from each of the six units. (b, c) Example of the time series of InSAR and ground reference shown for units 2 and 3, respectively.

The hydrograph of Unit 2 in the Sacramento Refuge showed a clear seasonal pattern with low water depths from April to October when wetlands were drawn down (Fig. 1(b)). Coherence data also showed a seasonal pattern with low and varying values in winter and spring when water depths were high, whereas coherence was relatively high and stable when water depth was low (shaded area in Fig. 1(b)), which was consistent with a previous study [14].

A. Reference pixel locations

By applying our automated method, we successfully found a reference point for each of the six units (Fig. 3(f)). The reference points were located close to the corresponding unit and were characterized by high coherence values in time and high phase connectivity with a coherent path to the unit. Note that we obtained multiple reference points for each unit and only showed the one with the shortest distance to the AOI.

The default threshold parameters worked for most of the units with some exceptions. We tuned *conn_perc_thd* from 0.8 to 0.75 for units 4 and 5, and additional tuning of *perc_thd* from 0.95 to 0.9 for unit 4 to be able to find a reference point. In addition, we applied a dilation of 2 pixels for units 1 and 3 in Step 5 to connect the unit to a close component (e.g., unit 3 and a nearby component in Fig. 3(e)).

B. Validation of InSAR estimated water depths

When estimating the time series of water depth, we set the starting date as the reference date for both InSAR and gauge water depth measurements (value of 0 for Fig.4(b), (c)). Considering a gauge is located at marginal places for each unit (Fig. 1(a)) with relatively high terrain elevation, we only used wetland pixels with lower elevation values of the DTM than the gauge's elevation and, therefore, the pixel locations were consistently flooded. We selected one representative wetland pixel for each unit with a relatively low RMSE to illustrate the results (Fig. 4). The water depth change from the selected wetland pixels was assumed to be the same as the changes in the gauge measurements considering a homogenous water surface for each small unit. The representative pixels from each of the units showed consistent InSAR results and ground reference with an R^2
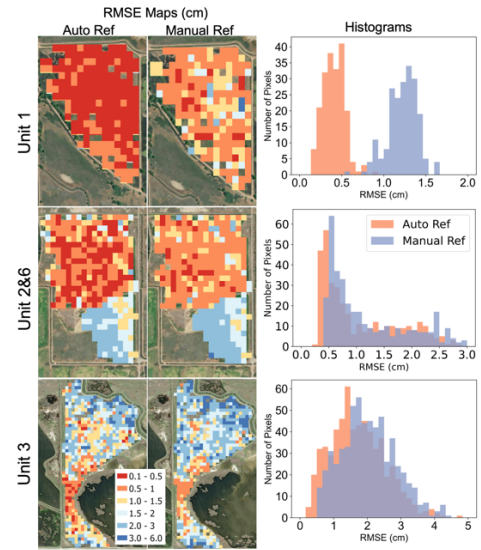

Fig. 5. Comparison of RMSE spatial distribution using the automatic and manually selected reference points.
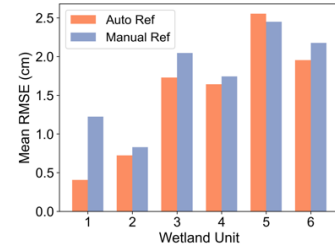

Fig. 6. Comparison of spatial average RMSE for six units using automatic and manually selected reference points.

value of 0.85 and RMSE of 0.77 cm (Fig. 4(a)) and time series results showed that InSAR successfully tracked draw-down of the flooding (Fig. 4(b), (c)). Overall, the average RMSE for all qualified wetland pixels in six units is 1.60cm using the automatic method and 1.82 cm for the manually selected reference point.

C. Comparison with the existing reference selection method

We compared the accuracy of predicted water depths for all six units between the automatic method (one reference for each unit) and a manually selected reference point method (one reference for all six units) (Fig. 5, 6). The manually selected point is in the western part of the study area and it was characterized by (1) concrete road with high coherence (95% of InSAR pairs with a coherence value greater than 0.90, Fig. 3(a)), (2) high-coherence pixels on the paths to all six units. We displayed the spatial distribution of RMSE for representative units (Fig. 5) and calculated for each unit the average of RMSE for all the pixels with elevation lower than the corresponding gauge elevation (Fig. 6).

The spatial distribution of RMSE of units 1, 2 & 6 (combined), and 3 clearly showed the advantage of using the algorithmically selected reference point compared to the manually selected point with lower RMSE values (Fig. 5). We used the Wilcoxon rank-sum statistical test to evaluate the difference among RMSE distributions resulting from the two methods and found that they were significantly different (Fig. 5, p-value < 0.05). Overall, the automatic approach

outperformed the manual selection for five out of six units, and only unit 5 showed a higher RMSE, which was close to the location of the manually selected point (Fig. 1(a)).

V. DISCUSSIONS AND CONCLUSIONS

Our study developed a method for automatically selecting optimal reference points for multi-temporal InSAR small baseline subsets analysis. We illustrated the effectiveness of the method by estimating long-term water depth variations in small, hydrologically distinct managed wetlands in the Sacramento National Wildlife Refuge, Central Valley, California. The five-step method evaluates coherence behavior and connectivity between a reference candidate to the AOI (wetland unit in this case). We tested the method on six wetland units, a landscape highly segmented by canals and levees as a challenging environment for InSAR analysis. The method successfully found optimal reference points for each of the units, which were used to generate accurate estimates of surface water depth.

When compared to the manually selected single reference, the automatic method with unit-based reference point selection achieved better results in five out of six units. The one with a slightly worse result (Unit 5 with 2.55 cm of RMSE for the automatic and 2.45 cm for the manual method) is characterized by a close distance to the location of the manually selected point and a coherent path (Fig. 3(a)). The manually selected point was also identified by the automatic method for Unit 5, whereas it ranked 20th due to a relatively longer distance to the AOI. Therefore, the automatic method does not necessarily result in better accuracy, but it achieves comparable accuracy to a manually selected point. For other studies with more complicated landscapes, there may not exist a single point with great phase connectivity to the AOIs and, thus, our method is expected to achieve better results.

One advantage of our method is to consider the coherent path between the reference point to the AOI. For example, our method outperformed the manually selected point for Unit 3 because there is no coherent path between the point and the unit (Fig. 3(e)), which introduced unwrapping errors that resulted in lower accuracy for the predicted water depths. Note that the manually selected point showed high connectivity to the AOI unit (Fig. 3(c), (d)) using the connected component generated by SNAPHU (data preparation step, Fig. 2(a)). We found that SNAPHU often showed that connected components included pixels with relatively low coherence values, which is partly due to the limit of the number of components. We successfully used a mask derived from the mean coherence to generate a new connected component that filters the reference candidates with coherent paths to the AOI to achieve better accuracy.

For future applications, users should adjust the selection parameters (Table 1) based on InSAR stack parameters and knowledge of local wetland environments. For example, the parameters in Table I correspond to connections with two nearest neighbors. If more connections are used in the stack processing, the threshold parameters *perc_thd* and *conn_perc_thd* should decrease accordingly. Also, users should tune other parameters, such as the *edge* parameter, to efficiently search for nearby reference candidates.

This new InSAR-based reference selection method not only has great potential for understanding regional wetland hydrology for other managed wetlands located in California with more complicated segmentation but also scientific value for other types of InSAR applications (e.g., landslide) in light of the upcoming NASA-ISRO SAR (NISAR).

CODE AVAILABILITY

The code was uploaded into the GitHub repository https://github.com/hippopaul/MyMintpy.

REFERENCES

[1] B. Zhang, S. Wdowinski, T. Oliver-Cabrera, R. Koirala, M. J. Jo, and B. Osmanoglu, "Mapping the extent and magnitude of sever flooding induced by Hurricane Irma with multi-temporal Sentinel-1 Sar and InSAR observations," ISPRS - Int. Arch. Photogramm. Remote Sens. Spat. Inf. Sci., vol. XLII–3, pp. 2237–2244, Apr. 2018.

[2] Z. Chen et al., "Characterizing marsh wetlands in the Great Lakes Basin with C-band InSAR observations," Remote Sens. Environ., vol. 242, p. 111750, Jun. 2020.

[3] H. Liao, S. Wdowinski, and S. Li, "Regional-scale hydrological monitoring of wetlands with Sentinel-1 InSAR observations: Case study of the South Florida Everglades," Remote Sens. Environ., vol. 251, p. 112051, Dec. 2020.

[4] B. Zhang, S. Wdowinski, D. Gann, S.-H. Hong, and J. Sah, "Spatio-temporal variations of wetland backscatter: The role of water depth and vegetation characteristics in Sentinel-1 dual-polarization SAR observations," Remote Sens. Environ., vol. 270, p. 112864, Mar. 2022.

[5] S.-H. Hong, S. Wdowinski, S.-W. Kim, and J.-S. Won, "Multi-temporal monitoring of wetland water levels in the Florida Everglades using interferometric synthetic aperture radar (InSAR)," Remote Sens. Environ., vol. 114, no. 11, pp. 2436–2447, Nov. 2010.

[6] T. Oliver-Cabrera, C. E. Jones, Z. Yunjun, and M. Simard, "InSAR Phase Unwrapping Error Correction for Rapid Repeat Measurements of Water Level Change in Wetlands," IEEE Trans. Geosci. Remote Sens., vol. 60, pp. 1–15, 2022.

[7] Y. Kang, Z. Lu, C. Zhao, Y. Xu, J.-W. Kim, and A. J. Gallegos, "InSAR monitoring of creeping landslides in mountainous regions: A case study in Eldorado National Forest, California," Remote Sens. Environ., vol. 258, p. 112400, Jun. 2021.

[8] Z. Yunjun, H. Fattahi, and F. Amelung, "Small baseline InSAR time series analysis: Unwrapping error correction and noise reduction," Comput. Geosci., vol. 133, p. 104331, Dec. 2019.

[9] D. Schaffer-Smith, J. J. Swenson, and M. E. Reiter, "Quantifying shorebird habitat in managed wetlands by modeling shallow water depth dynamics," Ecological, 2018.

[10] Central Valley Joint Venture (CVJV). 2020. Central Valley Joint Venture 2020 Implementation Plan. Sacramento, CA: U.S. Fish and Wildlife Service.

[11] P. A. Rosen, E. Gurrola, G. F. Sacco, and H. Zebker, "The InSAR scientific computing environment," in EUSAR 2012; 9th European Conference on SAR, VDE, Apr. 2012, pp. 730–733.

[12] H. Fattahi, P. Agram, and M. Simons, "A Network-Based Enhanced Spectral Diversity Approach for TOPS Time-Series Analysis," IEEE Trans. Geosci. Remote Sens., vol. 55, no. 2, pp. 777–786, Feb. 2017.

[13] C. W. Chen and H. A. Zebker, "Phase unwrapping for large SAR interferograms: statistical segmentation and generalized network models," IEEE Trans. Geosci. Remote Sens., vol. 40, no. 8, pp. 1709–1719, Aug. 2002.

[14] B. Zhang et al., "Multi-Temporal Analysis of InSAR Coherence, NDVI, and in Situ Water Depths for Managed Wetlands in National Wildlife Refuges, California," in IGARSS 2023 - 2023 IEEE, Jul. 2023, pp. 8186–8189.